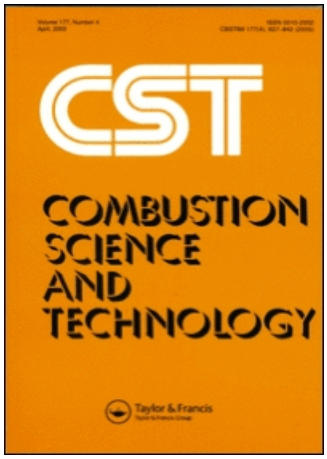

Combustion Science and Technology
Publication details, including instructions for authors and subscription information:
http://www.informaworld.com/smpp/title~content=t713456315

THE INFLUENCE OF REAL-GAS THERMODYNAMICS ON SIMULATIONS OF FREELY PROPAGATING FLAMES IN METHANE/OXYGEN/INERT MIXTURES

Online Publication Date: 01 September 2007
To cite this Article: Marchionni, Massimo, Aggarwal, Suresh K., Puri, Ishwar K. and Lentini, Diego (2007) 'THE INFLUENCE OF REAL-GAS THERMODYNAMICS ON SIMULATIONS OF FREELY PROPAGATING FLAMES IN METHANE/OXYGEN/INERT MIXTURES', Combustion Science and Technology, 179:9, 1777 - 1795
To link to this article: DOI: 10.1080/00102200701259999
URL: http://dx.doi.org/10.1080/00102200701259999

Combust. Sci. and Tech., 179: 1777–1795, 2007

ISSN: 0010-2202 print/1563-521X online
DOI: 10.1080/00102200701259999

The Influence of Real-Gas Thermodynamics on Simulations of Freely Propagating Flames in Methane/Oxygen/Inert Mixtures

Massimo Marchionni and Suresh K. Aggarwal
Department of Mechanical and Industrial Engineering,
University of Illinois at Chicago, Chicago, Illinois, USA

Ishwar K. Puri*
Department of Engineering Science and Mechanics,
Virginia Polytechnic Institute and State University,
Blacksburg, Virginia, USA

Diego Lentini
Dipartimento di Meccanica e Aeronautica, Università degli
Studi di Roma "La Sapienza," Rome, Italy

Abstract: The modeling of high-pressure combustion presents a continuing challenge in the context of chemical kinetics and mixture transport properties. This is mainly due to a lack of experimental data at high pressures. Consequently, there is limited confidence in the accuracy of simulations above moderate pressures. In this paper real gas thermodynamics is included in reacting flow simulations, e.g., by adopting the Redlich–Kwong equation of state, modifying the expression of the equilibrium reaction rate constants that are used to determine reverse reaction rates in a detailed reaction mechanism, and considering high-pressure effects on the enthalpy and specific heat. These real gas effects are characterized through simulations of freely propagating flames in methane/oxygen/inert mixtures at pressures up to 150 atm. Our results indicate that the

Received 19 July 2005; accepted 30 January 2007.
Extensive help provided by Professor P. Barry Butler (University of Iowa) for the modification of the CHEMKIN software to include real gas effects is greatly appreciated.
*Address correspondence to ikpuri@vt.edu

laminar flame speed decreases more rapidly with increasing pressure when the real gas formulation is employed than for an ideal gas, particularly for pressures greater than 40 atm. The differences can be ascribed to high-pressure effects on the mixture specific heat. The incorporation of real gas thermodynamics improves the agreement of predictions with measurements.

Keywords: Flame speed; Real-Gas thermodynamics; Subcritical combustion; Supercritical combustion

INTRODUCTION

Combustion modeling at higher pressures continues to face the challenge posed by a lack of experimental data and the unavailability of reliable chemistry and thermodynamic models. Apart from its fundamental relevance, high pressure combustion is important from practical considerations, since many applications operate at near critical and supercritical conditions, e.g., spark-ignition engines that typically operate at pressures around 60 atm, diesel engines around 120–150 atm, and gas turbines that can exceed 30 atm. Rocket engines, particularly those using liquid-propellants, operate at very high pressures, up to 250 atm and above. Therefore, there is a clear need to develop modeling capabilities to accurately simulate reacting flows at such high pressures.

Since the Reynolds number increases linearly with pressure, the reacting flow field is expected to be highly turbulent in most high-pressure combustion systems. However, inside the flame front, the flow is laminar at the finest scales, so that the role of chemistry becomes important. Table 1 presents the critical properties for CH_4, O_2, N_2 and He that form various methane/air/inert mixtures. Methane oxidation occurs in supercritical conditions at pressures above 50 atm. There are, however, conflicting opinions in the literature on the importance of real gas effects for phenomena occurring near and above the critical point. Simulations by Huang et al. (2004) show a 5% difference in ignition delay times predicted using the ideal gas and real gas formulations, for pressures up to 200 atm. However, Bellan (2000) suggested that the real gas approach should be employed for modeling slightly subcritical and supercritical fluid behavior and Zurbach et al. (2002) state a need for including

Table 1. Critical properties for the major species [Vargaftik, 1983]

Species	Critical pressure	Critical temperature
Methane	45.4 atm	191.1 K
Oxygen	49.8 atm	154.6 K
Nitrogen	33.5 atm	126.2 K
Helium	2.24 atm	5.19 K

real gas effects to simulate high-pressure methane/air combustion. Most reacting flow simulations at high pressures employ the ideal gas formulation, although real gas models have been developed for simulating high-pressure droplet vaporization (Jia and Gogos, 1993; Zhu and Aggarwal, 2000; Aggarwal et al., 2002; Zurbach et al., 2002), and combustion (Zurbach et al., 2002). Some recent investigations have considered real gas models for the simulation of constant-volume combustion (Schmitt et al., 1993) and ignition in homogeneous mixtures (Huang et al., 2004). However, these models have not been employed for flame propagation at high pressures.

While there have been significant advances in modeling reacting flows under atmospheric pressure, progress in developing simulation capabilities for high-pressure phenomena has been rather limited. This is primarily due to the difficulties in performing combustion experiments at the high pressures, and the lack of reliable high-pressure thermodynamic, transport and chemical kinetics models. For instance, the reaction mechanisms that are currently used for hydrogen-air (Tse et al., 2000; Kwon and Faeth, 2001) and methane-air (Hassan et al., 1998) mixtures have been validated only up to moderate pressures. Experimental data for individual species thermal conductivity at high pressure are very scarce, and in any case the evaluation of the mixture thermal conductivity requires a mixing rule, of uncertain definition. The situation is even worse for the species diffusion coefficients.

A better understanding of the influence of thermodynamic and transport properties and of the reaction chemistry is required at higher pressures. Herein, real gas thermodynamics has been incorporated to model high-pressure freely propagating premixed laminar flames. Real gas effects are included through the Redlich–Kwong equation of state and by modifying the expression of the equilibrium constants used to determine the reverse reaction rates. The real gas equation of state accounts for finite molecular dimensions and interactions between the molecules. Accordingly, a first modification to the ideal gas equation corrects for the volume available for the random movement of gas molecules, while a second reduces the molecular kinetic energy due to intermolecular attraction, which leads to a lower pressure as compared to an ideal gas. If the first effect dominates, the compressibility factor $Z > 1$ and the real gas density ρ^{RG} is smaller than ρ^{IG} for an ideal gas. If the second effect dominates, then $Z < 1$. Our aim is to characterize the pressures at which such effects are substantial. In addition, pressure effects on the enthalpy and specific heat are also considered. These high-pressure effects are quantified by simulating methane-air propagating flames at pressures up to 150 atm.

THE PHYSICAL AND NUMERICAL MODEL

The Sandia premixed flame code (Kee et al., 1999) is coupled with the CHEMKIN Real Gas Package (Schmitt et al., 1993) to simulate

freely propagating flames in methane/oxygen/inert mixtures at pressures up to 150 atm.

Conservation Equations

It is useful to revisit the equations governing the steady, isobaric, quasi-one-dimensional unstretched premixed flame propagation (Kee et al., 1999), namely,

$$\dot{M} = \rho u A \tag{1}$$

$$\dot{M}\frac{dT}{dx} - \frac{1}{c_p} - \frac{d}{dx}\left(\lambda A \frac{dT}{dx}\right) + \frac{A}{c_p}\sum_{k=1}^{K} \rho Y_k V_k c_{pk} \frac{dT}{dx} + \frac{A}{c_p}\sum_{k=1}^{K} \dot{\omega}_k h_k W_k = 0 \tag{2}$$

$$\dot{M}\frac{dY_k}{dx} + \frac{d}{dx}(\rho A Y_k V_k) - A\omega_k W_k = 0 \tag{3}$$

and for an ideal gas mixture

$$\rho^{IG} = \frac{p\overline{W}}{RT} \tag{4}$$

In these equations x denotes the spatial coordinate, $\dot{M}$ the mass flow rate, T the temperature, Y_k the molar fraction of kth species (there are K species), p the pressure, u the fluid mixture velocity, ρ the mass density, W_k the molecular weight of the kth species, $\overline{W}$ the mean mixture molecular weight, R the universal gas constant, λ the mixture thermal conductivity, c_p the constant pressure mixture specific heat, c_{pk} the counterpart for the kth species, $\dot{\omega}_k$ the molar chemical production rate of the kth species per unit volume, h_k its specific enthalpy, V_k its diffusion velocity, and A the cross-sectional area of the stream tube encompassing the flame.

Real Gas Thermodynamics

The Redlich–Kwong (R–K) cubic equation of state is adopted here. It is relatively simpler than other such relations, e.g., the Peng–Robinson or Becker–Kistiakowsky–Wilson equations, which require additional parameters (namely the acentric factor and binary-interaction coefficients, Reid et al., 1987; Schmitt et al., 1993; Annamalai and Puri, 2002). On the other hand, reliability of such a real gas model is questionable for some species such as helium or hydrogen. However, adopting a more refined state equation is inappropriate in the present context due to the fundamental uncertainties in other quantities crucial to the determination

of the flame propagation speed, e.g., thermal conductivity and species diffusion coefficients at high pressures.

Indeed, the flame propagation speed is determined by both chemical kinetics and thermal conductivity, as apparent from the Mallard–Le Chatelier (1883) dimensional relationship

$$S_L^0 \propto \sqrt{\alpha \frac{w}{\rho}} \tag{5}$$

α being the thermal diffusivity $\lambda/(\rho c_p)$, and w a representative species source term. Unfortunately, a universal expression for the thermal conductivity of a supercritical mixture is not available. Stiel and Thodos (1964) provide an expression for the thermal conductivity of a real gas in terms of the gas critical properties and of the reduced density (i.e., density over critical density). When the expression is compared with available experimental data, it shows modest qualitative agreement, e.g., for methane see Marchionni (2004), with the ratio of λ to its low-pressure counterpart increasing with pressure. However, its application to a *mixture* of real gases requires mixing rules to evaluate the mixture equivalent critical properties (see Yorizane et al., 1983; Reid et al., 1987). More important, the validity of Stiel and Thodos' relationship is limited to a reduced density less than 2.8, thus ruling out highly supercritical conditions of greater interest. As far as the species diffusion coefficients are concerned, correlations have been proposed for the self-diffusion coefficient of individual species, (Reid et al., 1987) for methane. However, a host of multicomponent diffusion coefficients are actually required for all species occurring in a reacting mixture in order to set up a reliable model; very little information is available about their values at high pressure. In the light of such uncertainties, λ and D_{ij} are left to their low-pressure expressions in the present investigation. Therefore, adopting a more elaborate real gas equation of state cannot substantially improve the reliability of the predictions. Accordingly, the Redlich–Kwong (R–K) equation is considered herein.

The R–K equation involves two parameters, namely, the critical pressure and temperature of species, where the critical properties have a physical meaning for stable species but not for radicals. The density is determined by evaluating the compressibility factor based on the R–K equation, i.e.,

$$p = \frac{RT}{(\bar{\nu} - \bar{b})} - \frac{\bar{a}}{T^{1/2}\bar{\nu}(\bar{\nu} - \bar{b})} \tag{6}$$

so that the real gas density

$$\rho^{RG} = \frac{\overline{W}}{\bar{\nu}} = \frac{\rho^{IG}}{Z} \tag{7}$$

can be based on the compressibility factor. Mixing rules can be used to evaluate the model constants (Reid et al., 1987; Schmitt et al., 1993; Annamalai and Puri, 2002). Mixing rules for quantities a and b, as well as expressions for caloric properties and equilibrium constants, see Eq. (9) and relevant discussion, are illustrated in the Appendix.

Detailed reaction mechanisms for combustion often provide Arrhenius rate constants for forward steps alone. The reverse rate of reaction j can be obtained using the equilibrium criteria

$$k_{rj} = \frac{k_{fj}}{K_{cj}} \tag{8}$$

where K_{cj} is the equilibrium "constant" for reaction j expressed in terms of molar concentration. This expression holds for both ideal and real gases, although K_{cj} is a function of temperature only for the former, but of both temperature and pressure for the latter. However, in the present implementation of CHEMKIN Real Gas (Schmitt et al., 1993), the equilibrium constant is expressed as

$$K_{cj} = K_{pj}^{IG}(T)\left(\frac{p_0}{ZRT}\right)^{\sum_{k=1}^{K}\Delta\nu_{kj}} \Big/ K_{\varphi j}(T,p) \tag{9}$$

where $K_{pj}^{IG}(T)$ is the ideal gas pressure-based equilibrium constant, $K_{\varphi j}(T,p)$ the real gas equilibrium constant in terms of fugacity coefficients, p_0 the reference pressure, and $\Delta\nu_{kj}$ the difference of the stoichiometric coefficients of species k in reaction j as a product and a reactant. Then, Eq. (9) requires the evaluation of the compressibility factor by a mixing rule, which in turn requires the composition to be specified, for which equilibrium values must be considered. CHEMKIN Real Gas uses the current composition (inevitably more or less removed from equilibrium) instead, with the underlying assumption that the accompanying error in estimating Z is small. This approximation calls for further investigation.

RESULTS AND DISCUSSION

In this Section, predictions by the present model are compared to available experimental data for the purpose of validation. The GRI Mech 3.0 chemical mechanism is employed, since it has been previously used to predict flame speeds and flame structure. Results using this mechanism are validated for pressures up to 40 atm by comparing our predictions with experimental data reported by Rozenchan et al. (2002). Figure 1 presents a comparison of predictions based on the real gas formulation with measurements of unstretched flame speeds for pressures up to 40 atm.

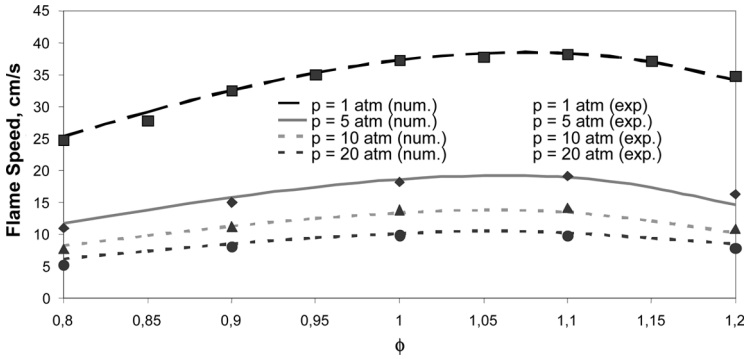

Figure 1. Comparison of measured (Rozechan et al., 2002) and predicted flame speeds vs equivalence ratio for methane-air mixtures, at four different pressures. Predictions based on the real gas model.

Excellent agreement between predictions and measurements is observed although for this range of pressures predictions based on the ideal gas formulation (not shown) are essentially identical to real gas results. The maximum flame speed for all cases occurs at an equivalence ratio $\phi \sim 1.1$, i.e., on the fuel rich side. The equivalence ratio at which flame speed peaks is determined by the competition between chemistry and diffusive transport. While the reaction rate decreases for both rich and lean mixtures as compared to stoichiometric, the thermal diffusivity is higher for rich mixtures; this accounts for the peak on the rich side.

Figure 2 compares the real gas predictions with both predicted and measured unstretched flame speeds for CH_4–O_2–He mixtures as reported by Rozenchan et al. (2002). The two conditions under scrutiny are for methane-oxidizer mixtures at 40 atm (with the oxidizer being a 17% O_2–83% He mixture) and 60 atm (15% O_2–85% He). Helium was used as a replacement for nitrogen in the experiments to increase the mixture Lewis number above unity so as to avoid flame front instabilities which would make evaluation of the unstreched flame speed from its stretched counterpart problematic. At 40 atm differences between simulations and measurements are lowest at $\phi \sim 0.9$, with the deviation being less than 1% for the real gas model, and over 4% for the ideal gas model. At higher pressures, and for leaner and richer mixtures, the differences between predictions and measurements become more significant, particularly for rich mixtures at 60 atm. This is likely due to deficiencies in the chemistry and transport models at these high pressures. Nonetheless, inclusion of real gas effects improves the accuracy of the predictions relative to those based on the ideal gas assumption. Unfortunately, no information is available about measurement uncertainties.

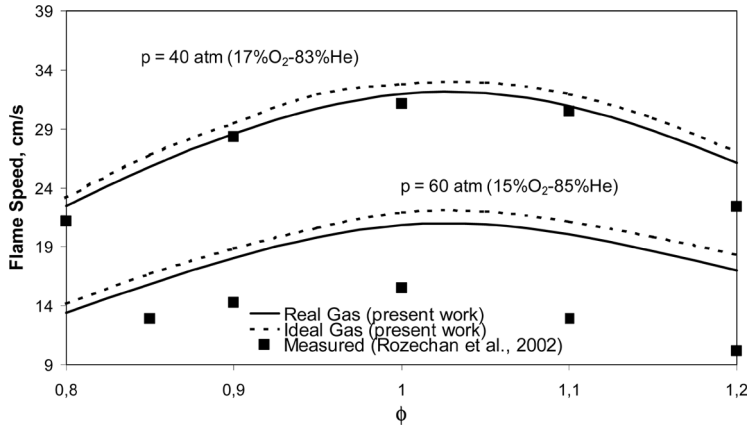

Figure 2. Comparison of measured (Rozechan et al., 2002) and predicted (both ideal and real gas models) flame speeds *vs* equivalence ratio for methane-oxygen-helium mixtures with (i) 17% O_2–83% He at 40 atm and (ii) 15% O_2–85% He at 60 atm.

Figure 3 presents predicted values of the unstretched flame speed with respect to pressure obtained using the ideal and real gas formulations for methane/air mixtures at $\phi = 1$ and 1.2 (initial temperature 298 K). There are negligible differences between the two models below 30 atm. For both models, the flame speed decreases rapidly with increasing pressure up to 30 atm, and then more slowly as the pressure increases up to 150 atm. The departure of the ideal gas model from its real gas counterpart increases with increasing pressure, with the former predicting higher flame speeds. At 50, 100 and 150 atm, these deviations are 6.4%, 10.5%, and 13%, respectively, for $\phi = 1$ flames, and 6.9%, 11.8%, and 14.9%, respectively, for $\phi = 1.2$. The inclusion of real gas effects lowers the predicted flame speed at high pressures, which can be ascribed to the pressure effect on the specific heat. This is further discussed below.

Figure 4 presents the temperature and CH_4 mole fraction profiles at 50 atm for a methane/air mixture at $\phi = 1$ that is analyzed using both the ideal and real gas models. The two sets of profiles are essentially indistinguishable. The corresponding profiles for two radical species (OH and CH) at 50 and 100 atm predicted using both the ideal and real gas models are presented in Figure 5. The differences between ideal and real gas predictions increase with pressure, with the real gas model predicting somewhat lower radical species concentrations. This suggests that inclusion of real gas effects lowers the flame speed by diminishing the radical pool. In general, the major scalar profiles are essentially uninfluenced by real gas effects, while minor species profiles are moderately influenced.

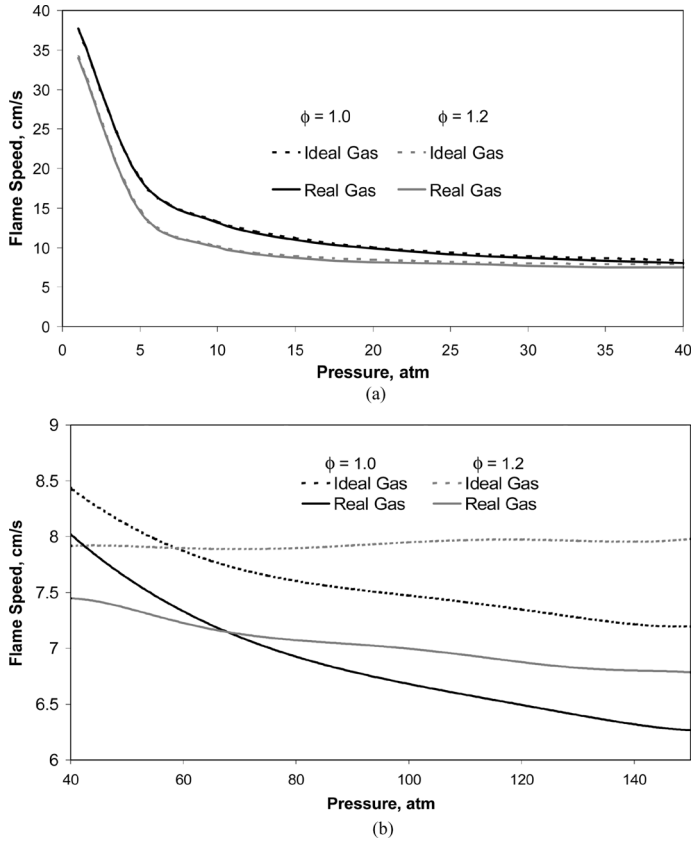

Figure 3. Flame speed *vs* pressure (both ideal and real gas models) methane/air mixtures at $\phi = 1$ and 1.2.

The experiments of Eberius and Kick (1992) demonstrate that the laminar flame speed for rich methane-air mixtures decreases monotonically as the pressure increases up to 100 atm (although their data are not corrected for stretch effects). Instead, the flame speed predicted using the *ideal* gas model exhibits, as shown in Figure 6, a non-monotonic behavior with respect to pressure for rich mixtures ($\phi = 1.15$ and 1.2) in contrast to that for stoichiometric and lean mixtures. The ideal gas approach overestimates both the thermal diffusivity and the reaction rate (see below); this leads to overestimated flame speeds at high pressure, giving rise to the non-monotonic behavior. Using the real gas model removes this discrepancy, as shown in Figure 3b.

The unstretched flame speed can be expressed through the Mallard–Le Chatelier functional relation of Eq. (5). According to this expression,

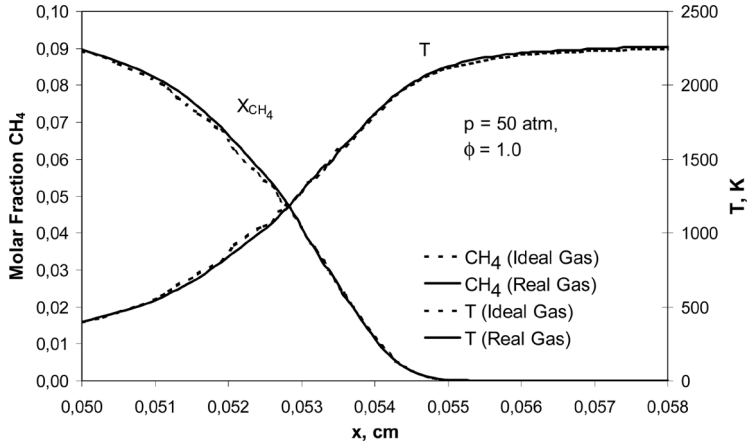

Figure 4. Temperature and methane molar fraction profiles (both ideal and real gas models) for a stoichiometric methane-air mixture at 50 atm.

the decrease in flame speed with pressure occurs due to the effect of pressure on the thermal diffusivity, which is influenced by real gas effects since $\alpha = \lambda/(\rho c_p)$ where all factors depend on p, and on the reaction rate. Figure 7 shows the variation of the quantities c_p^* and α^* with pressure (for $\phi = 1.2$). They are defined as

$$c_p^* = c_p^{RG}/c_p^{IG} \quad \text{and} \quad \alpha^* = \alpha^{RG}/\alpha^{IG} \approx Z/c_p^*. \tag{10}$$

The second equality in Eq. (10) is based on the assumption that λ is independent of p. The first of these relations addresses real gas effects on the specific heat while the latter also includes effects due to thermal diffusivity. The figure reports values determined at a position in the flame where the local temperature is 400 K.

As shown in Figure 7, the value of α^* decreases because c_p^* increases with pressure. The value of Z in this range is smaller than 1.02, which is in agreement with the measured values for methane-air mixtures reported by Vargaftik (1983). The dominant effect is due to the specific heat. The issue is further investigated by considering three dimensionless parameters that are also computed at the location where the local temperature is 400 K, namely,

$$\rho' = \rho^{RG}/\rho^{IG} = 1/Z, \; c_p' = c_p(p)/c_{p,0}, \quad \text{and} \quad \dot{\omega}'_{CH_4} = \dot{\omega}'_{CH_4}(p)/\dot{\omega}'_{CH_4,0} \tag{11}$$

Here the subscript 0 implies atmospheric pressure conditions. Examining the effect of pressure on these parameters for both the ideal and real gas models helps to further understand real gas effects. The first of these

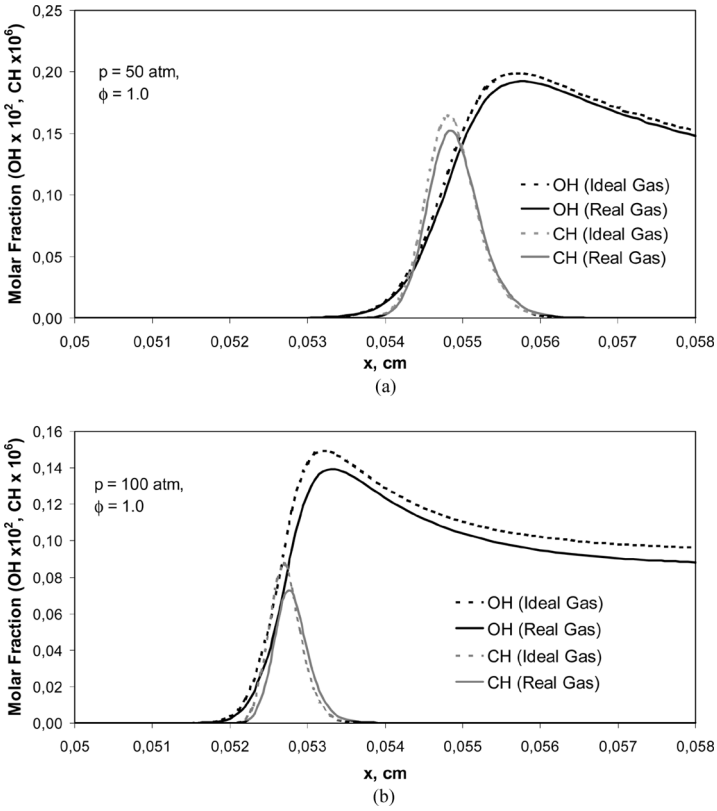

Figure 5. Predicted OH and CH species profiles (both ideal and real gas models) for stoichiometric methane-air mixtures at 50 and 100 atm.

parameters deviates from unity by less than 2% up to 150 atm for the $\phi = 1$ and 1.2 flames, in agreement with Figure 7, with the real gas density smaller than that of the corresponding ideal gas. This is reasonable for the current reduced temperature (i.e., ratio of the local temperature to the critical value) of 2.9, which is higher then the Curie temperature (2.76) at which a gas begins to behave as ideal (Annamalai and Puri, 2002). In addition, the non-dimensional reaction rate parameter $\omega^*_{CH4} = \omega^{RG}_{CH4}/\omega^{IG}_{CH4}$ is smaller than unity in the pressure range from 1–150 atm (also see later). Hence, the predicted flame speed using the real gas model is smaller than for a corresponding ideal gas.

Figure 8 presents the molar production rate (normalized with respect to the atmospheric value) behavior with respect to pressure based on both the ideal and real gas models for the $\phi = 1$ and 1.2 flames. At 50 atm, the values for stoichiometric flames are about three times larger than at

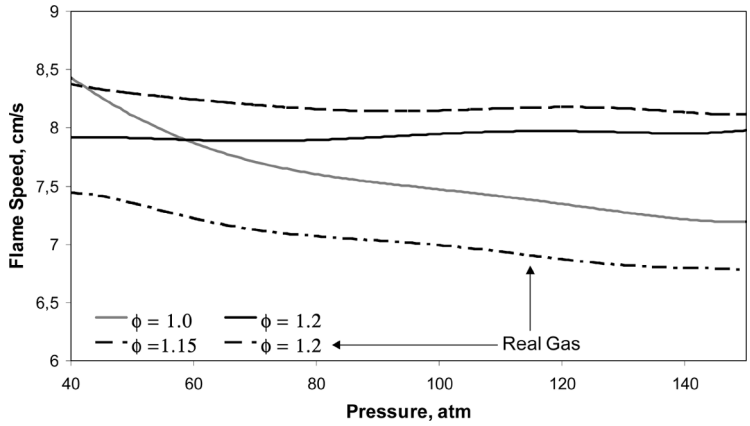

Figure 6. Predicted laminar flame speed as a function of pressure for methane-air mixtures at $\phi = 1.0$, 1.15 and 1.2 (using the ideal gas formulation), and at $\phi = 1.2$ (real gas formulation).

atmospheric conditions for both models; at 100 atm both the ratios are roughly eightfold; and at 150 atm these ratios are 18.6 and 16.9 for ideal and real gas mixtures, respectively. For the fuel-rich flame, both ratios are smaller than three up to 60 atm, after which they show a steep increase reaching values of 19.3 (ideal gas) and 21.1 (real gas) at 150 atm. These differences between ideal and real gas results imply that changes in chemistry due to different thermodynamic assumptions have

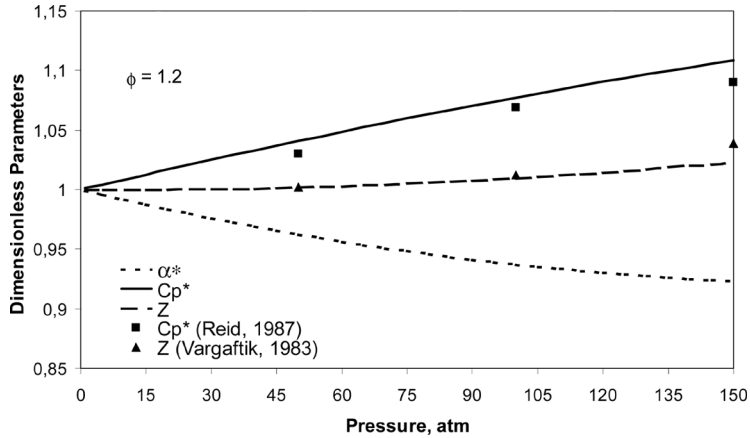

Figure 7. Variation of dimensionless parameters α^*, c_p^* and Z with pressure for a methane-air mixture at $\phi = 1.2$. Predictions in present work are compared with estimated values by Reid et al. (1987) for c_p^*, and with a value determined from experimental data (Vargaftik, 1983) for Z.

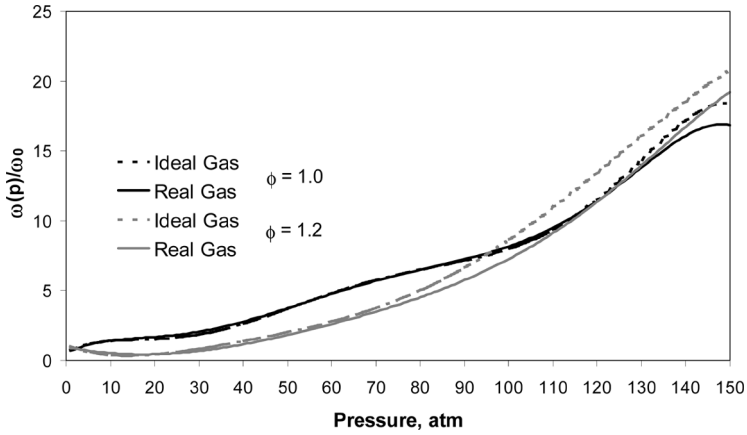

Figure 8. Variation of dimensionless parameter $\dot{\omega}_{CH_4}(p)/\dot{\omega}'_{CH_4,0}$ with pressure (both ideal and real gas models) for methane-air mixtures at $\phi = 1.0$ and 1.2.

as significant an influence on the flame speed as the thermal diffusivity α. For an ideal gas mixture the specific heat is pressure-independent but for a real gas it increases with pressure. There is satisfactory agreement for the quantity $(c_p - c_p^0)/R$ (for $\phi = 1$ and 1.2 mixtures at 400 K) based on the real gas model and data reported by Reid et al. (1987). Figure 9 presents the variation of c_p with pressure for the $\phi = 1.2$ flame, which is similar to that for $\phi = 1$ (not shown).

As already noted, the behavior of the flame speed with increasing pressure is influenced by a competition between two effects, heat conduction and the reaction rate, as is apparent from Eq. (5). In a

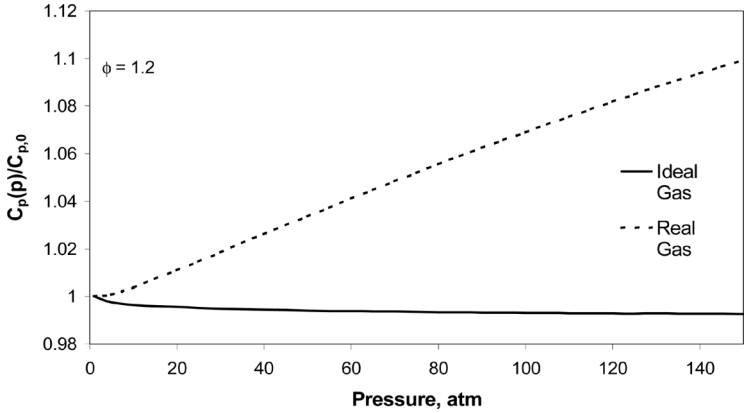

Figure 9. Variation of dimensionless parameter c'_p with pressure (both ideal and real gas models) for a methane-air mixture at $\phi = 1.2$.

premixed flame, the burned gases heat the incoming fresh reactants. This process is strongly influenced by the value of α, which is the ratio of the transported to the absorbed heat flux. Within the present assumptions, the effect of pressure on thermal conductivity is not considered. Increasing pressure influences the energy absorption through the larger mixture density, which leads to a larger absorbing mass. At 400 K for reactive methane-air mixture a real gas model predicts a smaller density than the ideal case as well as a higher specific heat. The net result is that, in the present case, α turns out to be smaller for the real gas model as compared to an ideal gas, thus contributing to a lower flame speed.

The behavior of the overall reaction rate with increasing pressure can be related to pressure as

$$\dot{\omega} \propto p^n \tag{12}$$

where n denotes the overall reaction order. The larger the overall reaction order, the greater the influence of pressure on the chemistry. Since the overall reaction order decreases for pressures up to 5 atm due to a competition between the termination reactions

$$H + O_2 + M \rightarrow HO_2 + M \tag{13}$$

and

$$H + CH_3(+M) \rightarrow CH_4(+M) \tag{14}$$

and the major branching reaction

$$H + O_2 \rightarrow O + OH \tag{15}$$

the reaction rate increases only weakly for pressures below 5 atm. In this range, the dominant process influencing the flame speed is the decreasing thermal diffusivity. Hence, the flame speed for a stoichiometric mixture decreases from about 38 cm/s at 1 atm to 18 cm/s at 5 atm, where n reaches a minimum. As the pressure increases further, another branching reaction,

$$HO_2 + CH_3 \rightarrow OH + CH_3O \tag{16}$$

becomes relatively important and is responsible for an increase in the value of n. This reaction supplies the flame with OH radicals required by the chain propagation reaction (Rozechan et al., 2002)

$$OH + CO \rightarrow H + CO_2 \tag{17}$$

This always applies irrespective of use of the real or ideal gas models.

The consequent increase in the reaction order contributes to a higher reaction rate, which partly compensates for the decay in the thermal

diffusivity. This counterbalance moderates the flame speed decrease, from 13.2 cm/s at 10 atm down to 6.8 cm/s at 100 atm for $\phi = 1.0$ when the real gas formulation is applied. The discrepancies between our predictions and the experimental data can be ascribed to inaccuracies in the models for chemical kinetics and transport properties that are used herein. At any rate, the real gas formulation represents in this regard an improved model for caloric properties.

Figure 10 shows the temperature profiles for stoichiometric methane-air flames predicted by the real gas model at 50, 100 and 150 atm. The data show that the flame thickness decreases with pressure due to compression. This decrease is also apparent through the concentration profiles of OH and CH radicals shown in Figure 11. As expected, the profiles indicate that both the peak and equilibrium values of radical species concentrations decrease with pressure. Although compression increases the species concentrations available for chemical reactions, it also increases the role of recombination reactions. An important implication here is that the reduction in the flame speed is also related to the observed depletion of the radical pool when real gas effects are taken into account.

The lack of strong wrinkling in methane-air flames, experimentally observed at high pressures, Rozenchan et al. (2002) (in contrast to hydrogen-air flames, Rozenchan, 2001), is due to their larger flame thickness. Flames burning methane self-accelerate and transition to turbulence or a detonation wave at relatively higher pressures than hydrogen flames do. As the flame speed increases, the characteristic propagation time, which is a convective time, is significantly reduced. If the characteristic time were to be smaller than the diffusion time, the flame would transition into a convection-dominated detonation wave or into a turbulent

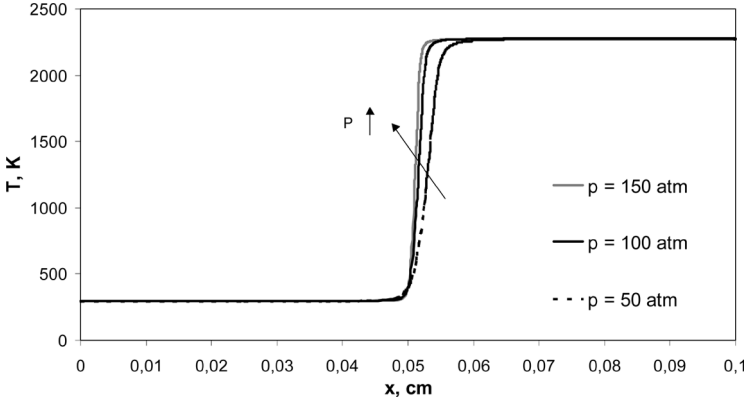

Figure 10. Predicted temperatures profiles (real gas model) for a stoichiometric methane-air mixture at 50, 100 and 150 atm (reactant temperature 298 K).

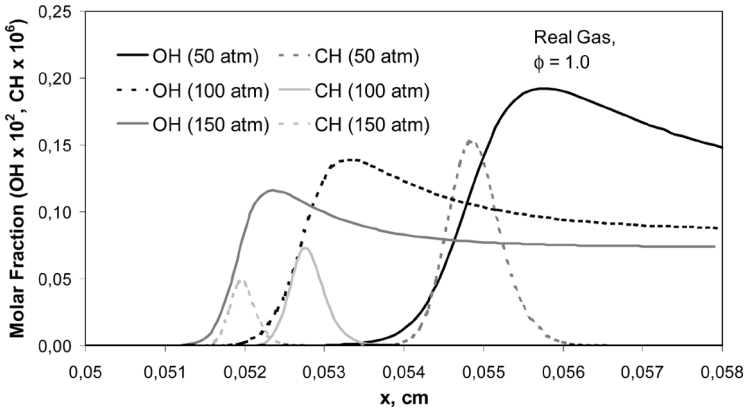

Figure 11. Predicted OH and CH mole fraction profiles, same conditions as in Figure 10.

flame, depending on the initial volume (Rozenchan et al., 2002).At 150 atm, the flame thickness is an order of magnitude smaller than at atmospheric pressure, thereby indicating that such a transition might occur more readily at higher pressures.

CONCLUSIONS

In the present study, real gas thermodynamics have been incorporated in reacting flow simulations. The real gas effects accounted for include the Redlich-Kwong equation of state, the modification of the equilibrium reaction rate constants that are used to compute reverse reaction rates in the detailed reaction mechanism, and the pressure effects on enthalpy and specific heat.

Our results indicate that for pressures below 40 atm, the unstretched laminar flame speeds for methane-air mixtures predicted using the ideal gas and real gas models are essentially identical. The predicted flame structures are also essentially the same for the two models, implying that the real gas effects are negligible for pressures below this pressure level. For pressures above 40 atm, the predicted laminar flame speeds decrease more rapidly with increasing pressure when the real gas formulation is employed, which improves the agreement with measurements.

Real gas effects on premixed flames appear mainly through their influence on the specific heat, which increases with pressure. This effect decreases the thermal diffusivity, and thereby decreases the laminar speed as compared to ideal gas predictions. The inclusion of real gas thermodynamics is found to have a negligible effect on the mixture density, since the compressibility

factor increases by only about 2% as the pressure is increased to 150 atm. For pressures up to 150 atm, there is a relatively small effect of including real gas thermodynamics on the premixed flame structure. While the temperature and major species profiles computed using the real gas and ideal gas models exhibit small differences, the radical species profiles show relatively larger differences. The real gas model predicts lower radical species concentrations compared to those predicted using the ideal gas model.

The development of more reliable models for high-pressure combustion requires a more consistent evaluation of the equilibrium constants used to recover reverse reaction rates, and, more fundamentally, the inclusion of real gas departure functions for transport effects, namely thermal conductivity and species diffusivities.

REFERENCES

Aggarwal, S.K., Yan, C., and Zhu, G. (2002) Transcritical vaporization of a liquid fuel droplet in a supercritical ambient. *Combust. Sci. Tech.*, **174**, 103–130.

Annamalai, K. and Puri, I.K. (2002) Advanced Thermodynamics Engineering, CRC Press, Boca Raton, FL.

Bellan, J. (2000) Supercritical (and subcritical) fluid behavior and modeling: drops, streams, shear and mixing layers, jets and sprays. *Prog. Energy Combust. Sci.*, **26**, 329.

Eberius, H. and Kick, T. (1992) Stabilization of premixed, conical methane flames at high pressure. *Ber. Bunsen-Ges. Phys. Chem.*, **96**, 1416.

Hassan, M.I., Aung, K.T., and Faeth, G.M. (1998) Measured and predicted properties of laminar premixed methane/air flames at various pressures. *Combust. Flame*, **115**, 539.

Huang, J., Hill, P.G., Busche, W.K., and Munshi, S.R. (2004) Shock-tube study of methane ignition under engine-relevant conditions: experiments and modeling. *Combust. Flame*, **136**, 25.

Jia, H. and Gogos, G. (1993) High pressure droplet vaporization; effects of liquid gas solubility. *Int. J. Heat Mass Trans.*, **36**, 4419.

Kee, R.J., Rupley, F.M., Miller, J.A., Coltrin, M.E., Grcar, J.F., Meeks, E., Moffat, H.K., Lutz, A.E., Dixon-Lewis, G., Smooke, M.D., Warnatz, J., Evans, G.H., Larson, R.S., Mitchel, R.E., Petzold, R.L., Reynolds, W.C., Caracotios, M., Steward, W.E., and Glarborg, P. (1999) PREMIX, a Fortran Program for Modeling Steady, Laminar, One-Dimensional Premixed Flames, *Technical Report* Pre-035-1 CHEMKIN Collection Release 3.5, Reaction Design Inc., San Diego, CA.

Kwon, O.C. and Faeth, G.M. (2001) Flame/stretch interactions of premixed hydrogen-fueled flames: Measurements and predictions. *Combust. Flame*, **124**, 590.

Mallard, E. and Le Chatelier, H.L. (1883) Recherches expérimentales et théoriques sur la combustion des mélanges gazeux explosifs. *Ann. Minnes*, **8**, 274.

Marchionni, M. (2004) Modellizzazione di gas reale e soluzioni numeriche per la propagazione di fiamme premiscelate ad alta pressione. MS Thesis in Aerospace Engineering, Università degli Studi di Roma "La Sapienza".

Reid, R.C., Prausnitz, J.M., and Poling, B.E. (1987) The properties of gases and liquids, 4th ed., McGraw-Hill, New York.

Rozenchan, G. (2001) An Experimental Study of Outwardly-Propagating Hydrogen and Flames at High Pressures, MS Thesis, Princeton University.

Rozenchan, G., Zhu, D.L., Law, C.K., and Tse, S.D. (2002) Outward propagation, burning velocities, and chemical effects of methane flames up to 60 atm. *Proc. Combust. Inst.*, **29**, 1461.

Schmitt, R.G., Butler, P.B., and French, N.B. (1993) CHEMKIN REAL GAS: A fortran package for analysis of thermodynamics properties and chemical kinetics in non-ideal systems. CHEMKIN Real Gas User's Guide, University of Iowa.

Stiel, L.I. and Thodos, G. (1964) The thermal conductivity of nonpolar substances in the dense gaseous and liquid regions. *AICHE J.*, **10**, 266.

Tse, S.D., Zhu, D.L., and Law, C.K. (2000) Morphology and burning rates of expanding spherical flames in H_2/O_2/inert mixtures up to 60 atmospheres. *Proc. Combust. Instit.*, **28**, 1793.

Vargaftik, N.B. (1983) Handbook of Physical Properties of Liquid and Gases, 2nd ed., Hemisphere, New York.

Yorizane, M., Yoshimura, S., Masuoka, H., and Yoshida, H. (1983) Thermal conductivity of binary gas mixture at high pressures: N_2-O_2, N_2-Ar, CO_2-Ar and CO_2-CH_4. *Ind. Eng. Chem. Fund.*, **22**, 458.

Zhu, G.S. and Aggarwal, S.K. (2000) Transient supercritical droplet vaporization with emphasis on the effects of equation of state. *Int. J. Heat Mass Transfer*, **43**, 1157.

Zurbach, S., Thomas, J.L., Vuillermoz, P., Vingert, L., and Habiballah, M. (2002) Recent Advances on LOX/Methane Combustion for Liquid Rocket Engine Injector, AIAA paper 2002–4321.

APPENDIX

Terms a and b of the R–K equation are computed, for each species, after its critical properties as follows:

$$a_i = \frac{27\,R^2 T_{c,i}}{64\,p_{c,i}} \tag{A1}$$

$$b_i = \frac{R T_{c,i}}{8\,p_{c,i}} \tag{A2}$$

Then, in oder to compute the mixture compressibility factor, the following mixing rules apply (X_i denoting molar fraction):

$$a = \sum_i^K \sum_j^K X_i X_j \sqrt{a_i a_j} \tag{A3}$$

$$b = \sum_{i}^{K} X_i b_j \tag{A4}$$

Concerning the energy balance, ideal gas properties (specific heat and enthalpy) of individual species are computed from NASA polynomials. The mixture properties are then computed following mixing rule (A4) with c_p and h respectively instead of b. When using the R–K equation of state, real gas effects are taken in account by introducing the departure function defined as follows (expression applicable to mixture only):

$$H^{RG} - H^{IG} = RT(Z-1) + \int_{V}^{\infty} \left(p - T \frac{\partial p}{\partial T}\bigg|_{V} \right) dV \tag{A5}$$

In addition to the above expression real gas effects are introduced in the mixture constant pressure specific heat computation as (the subscript n denoting fixed composition):

$$c_p^{RG} = \frac{\partial H}{\partial T}\bigg|_{p,n} = c_p^{IG} + \frac{\partial}{\partial T}[H^{RG} - H^{IG}]\bigg|_{p,n} \tag{A6}$$

For the kth reaction, the pressure-based equilibrium constant for an ideal gas is computed following the expression

$$K_{p,k} = \exp\left(\sum_{i}^{K} \Delta\nu_{k,i} \left(\frac{s_i}{R} - \frac{h_i}{RT} \right) \right) \tag{A7}$$

which is used in Eq. (9) to get the equivalent property for real gases.